A Trio of 40 to 50 Million Year Old Mini-Neptunes from Kepler, TESS, and Gaia

L. G. BOUMA,[1,] [*] R. KERR,[2] J. L. CURTIS,[3,4] H. ISAACSON,[5] L. A. HILLENBRAND,[1] A. W. HOWARD,[1] A. L. KRAUS,[2] A. BIERYLA,[6]
D. W. LATHAM,[6] E. A. PETIGURA,[7] AND D. HUBER[8]

[1]*Cahill Center for Astrophysics, California Institute of Technology, Pasadena, CA 91125, USA*
[2]*Department of Astronomy, The University of Texas at Austin, Austin, TX 78712, USA*
[3]*Department of Astronomy, Columbia University, 550 West 120th Street, New York, NY 10027, USA*
[4]*Department of Astrophysics, American Museum of Natural History, New York, NY 10024, USA*
[5]*Astronomy Department, University of California, Berkeley, CA 94720, USA*
[6]*Center for Astrophysics | Harvard & Smithsonian, 60 Garden St, Cambridge, MA 02138, USA*
[7]*Department of Physics & Astronomy, University of California Los Angeles, Los Angeles, CA 90095, USA*
[8]*Institute for Astronomy, University of Hawaii, 2680 Woodlawn Drive, Honolulu, HI 96822, USA*

ABSTRACT

Stellar positions and velocities from Gaia are yielding a new and refined view of open cluster dispersal. Here we present an analysis of a group stars spanning Cepheus ($l = 100°$) to Hercules ($l = 40°$), hereafter the Cep-Her complex. The group includes four Kepler Objects of Interest: Kepler-1643 b ($R_\mathrm{p} = 2.32 \pm 0.14\,R_\oplus$, $P = 5.3$ days), KOI-7368 b ($R_\mathrm{p} = 2.22 \pm 0.12\,R_\oplus$, $P = 6.8$ days), KOI-7913 Ab ($R_\mathrm{p} = 2.34 \pm 0.18\,R_\oplus$, $P = 24.2$ days), and Kepler-1627 Ab ($R_\mathrm{p} = 3.85 \pm 0.11\,R_\oplus$, $P = 7.2$ days). The latter Neptune-sized planet is in a sub-component of the Cep-Her complex called the δ Lyr cluster (Bouma et al. 2022). Here we focus on the former three systems, which are in other sub-components of the complex. Based on kinematic evidence from Gaia, stellar rotation periods from TESS, and spectroscopy, these three systems are also $\approx$40 million years old. More specifically, we find that Kepler-1643 is in a dense sub-cluster of the complex called RSG-5, and is 46^{+9}_{-7} Myr old. KOI-7368 and KOI-7913 are in a diffuse region that we call CH-2, and are 36^{+10}_{-8} Myr old. Based on the transit shapes and high resolution imaging, all three are most likely planets, with false positive probabilities of 6×10^{-9}, 4×10^{-3}, and 1×10^{-4} for Kepler-1643, KOI-7368, and KOI-7913 respectively. These planets therefore empirically demonstrate that mini-Neptunes with sizes of $\approx$2 Earth radii exist at ages of $\approx$40 million years.

1. INTRODUCTION

The discovery and characterization of transiting planets younger than a billion years is a major frontier in current exoplanet research. The reason is that the properties of young planets provide benchmarks for studies of planetary evolution. For instance, there are the questions of when hot Jupiters arrive on their close-in orbits (Dawson & Johnson 2018), how the sizes of planets with massive gaseous envelopes evolve (Rizzuto et al. 2020), when and if close-in multiplanet systems fall out of resonance (Arevalo et al. 2022; Goldberg & Batygin 2022), and whether and how

Corresponding author: L. G. Bouma
luke@astro.caltech.edu

[*] 51 Pegasi b Fellow

mass-loss explains the radius valley (Lopez et al. 2012; Owen & Wu 2013; Fulton et al. 2017; Ginzburg et al. 2018; Lee & Connors 2021).

The discovery of a young planet requires two claims to be fulfilled: the planet must exist, and its age must be secured. Spaced-based photometry from K2 and TESS has yielded a number of young planets for which the planetary evidence comes from transits, and the age evidence is based on either cluster membership (Mann et al. 2017; David et al. 2019; Newton et al. 2019; Bouma et al. 2020; Nardiello et al. 2020) or else on correlates of youth such as stellar rotation, photospheric lithium abundances, x-ray activity, or emission line strength (Zhou et al. 2021; Hedges et al. 2021).

In this work, we leverage recent analyses of the Gaia data, which have greatly expanded our knowledge of stellar group memberships (*e.g.*, Cantat-Gaudin et al. 2018; Kounkel & Covey 2019; Kerr et al. 2021). To date these analyses have

mostly clustered on the stellar positions and on-sky velocities measured by Gaia, with varying degrees of filtering and supervision. One important result is the identification of diffuse streams and tidal tails comparable in stellar mass to the previously known cores of nearby open clusters (Meingast et al. 2019; Meingast et al. 2021; Gagné et al. 2021). These spatially diffuse groups typically have velocity dispersions of $\approx 1\,\mathrm{km\,s^{-1}}$, though they can be much higher due to both projection effects and internal dynamics. As an extreme example, in the Hyades the velocities of stars in the tidal tails are thought to span up to $\pm 40\,\mathrm{km\,s^{-1}}$ relative to the cluster center (Jerabkova et al. 2021). The stars in such diffuse regions can be verified to be the same age as the core members (*i.e.*, coeval) through analyses of color-absolute magnitude diagrams, stellar rotation periods (Curtis et al. 2019; Bouma et al. 2021), and chemical abundances (Hawkins et al. 2020). While there are many implications for our understanding of star formation and cluster evolution (Dinnbier & Kroupa 2020), a more immediate consequence is that we now know the ages of many more stars, including previously known planet hosts.

The prime Kepler mission (Borucki et al. 2010) found most of the currently known transiting exoplanets, and it was conducted before Gaia. It therefore seems sensible to revisit the Kepler field, given our new knowlege of the stellar ages.

In this work, we expand on our previous study of a 38^{+7}_{-6} million year old Neptune-sized planet in the Kepler field (Kepler-1627 Ab; Bouma et al. 2022). The age of this planet was derived based on its host star's membership in the δ Lyr cluster. Our analysis of the cluster focused on the immediate spatial and kinematic vicinity of Kepler-1627 A in order to confirm the age of the planet. However it became clear that the δ Lyr cluster seems to also be part of a much larger group of similarly aged stars. This group, which is at a distance of $\sim 330\,\mathrm{pc}$ from the Sun, appears to span Cepheus to Hercules (galactic longitudes, l, between $40°$ and $100°$), at galactic latitudes roughly between $0°$ and $20°$. We therefore refer to it as the Cep-Her complex. It exhibits significant substructure over its ≈ 250 parsec length, and a detailed analysis of its memberships, kinematics, and possible origin is currently being prepared by R. Kerr and collaborators.

Here, our focus is on the intersection of the Cep-Her complex with the Kepler field. Cross-matching the full set of candidate Cep-Her members against known Kepler Objects of Interest (KOIs) (Thompson et al. 2018) yielded four candidate cluster members: Kepler-1627, Kepler-1643, KOI-7368, and KOI-7913. Given our previous analysis of Kepler-1627, we will mostly focus on the latter three. After analyzing the relevant properties of Cep-Her (Section 2), we derive the stellar properties (Section 3) and validate the planetary nature of each system using a combination of the Kepler photometry and high-resolution imaging (Section 4). We conclude with a few caveats, and discuss implications for the size-evolution of close-in mini-Neptunes (Section 5).

2. THE CEP-HER COMPLEX

2.1. *Previous Related Work*

Our focus is on a region of the Galaxy approximately 200 to 500 pc from the Sun, above the galactic plane, and spanning galactic longitudes of roughly $40°$ to $100°$ degrees. Two rich clusters in this region are the δ Lyra cluster (Stephenson 1959) and RSG-5 (Röser et al. 2016). Each of these clusters was known before Gaia. They have reported ages between ≈ 30 and ≈ 60 million years. Early empirical evidence that these two clusters could be part of a large and more diffuse population was apparent in the Gaia-based photometric analysis of pre-main-sequence stars by Zari et al. (2018, see their Figures 11 and 13). Further kinematic connections and complexity were highlighted by Kounkel & Covey (2019), who included these previously known groups in the larger structures dubbed "Theia 73" and "Theia 96"[1]. The connection made by Kounkel & Covey (2019) between the previously known open clusters and the other groups in the region was made as part of an unsupervised clustering analysis of the Gaia DR2 positions and tangential velocities with a subsequent manual "stitching" step, and generally supports the idea that there is an overdensity of ≈ 30 and ≈ 60 million year old stars in this region of the Galaxy. Kerr et al. (2021), in a volume-limited analysis of the Gaia DR2 point-source catalog out to one third of a kiloparsec, identified three of the nearest sub-populations, dubbed "Cepheus-Cygnus", "Lyra", and "Cerberus". Kerr et al. (2021) reported ages for each of these subgroups between 30 and 35 million years.

2.2. *Member Selection*

The possibility that the δ Lyr cluster, RSG-5, and the subpopulations identified by Kerr et al. (2021) share a common origin has yet to be fully substantiated, and will be the subject of the upcoming study by R. Kerr and collaborators. Our primary interest in the region stems from the fact that a portion of it was observed by Kepler (Figure 1, top panel). To further explore the population of stars that were observed, we select candidate Cep-Her members through four steps, the first three being identical to those described in Section 3 of Kerr et al. (2021). We briefly summarize them here.

The first step is to select stars that are photometrically distinct from the field star population based on Gaia EDR3 magnitudes $\{G, G_{\mathrm{RP}}, G_{\mathrm{BP}}\}$, parallaxes and auxiliary reddening estimates (Lallement et al. 2019). This step yielded 1097 stars with high-quality photometric and astrometry, which are either pre-main-sequence K and M dwarfs due to their

---

[1] See their visualization online at http://mkounkel.com/mw3d/mw2d.html (accessed 15 March 2022)
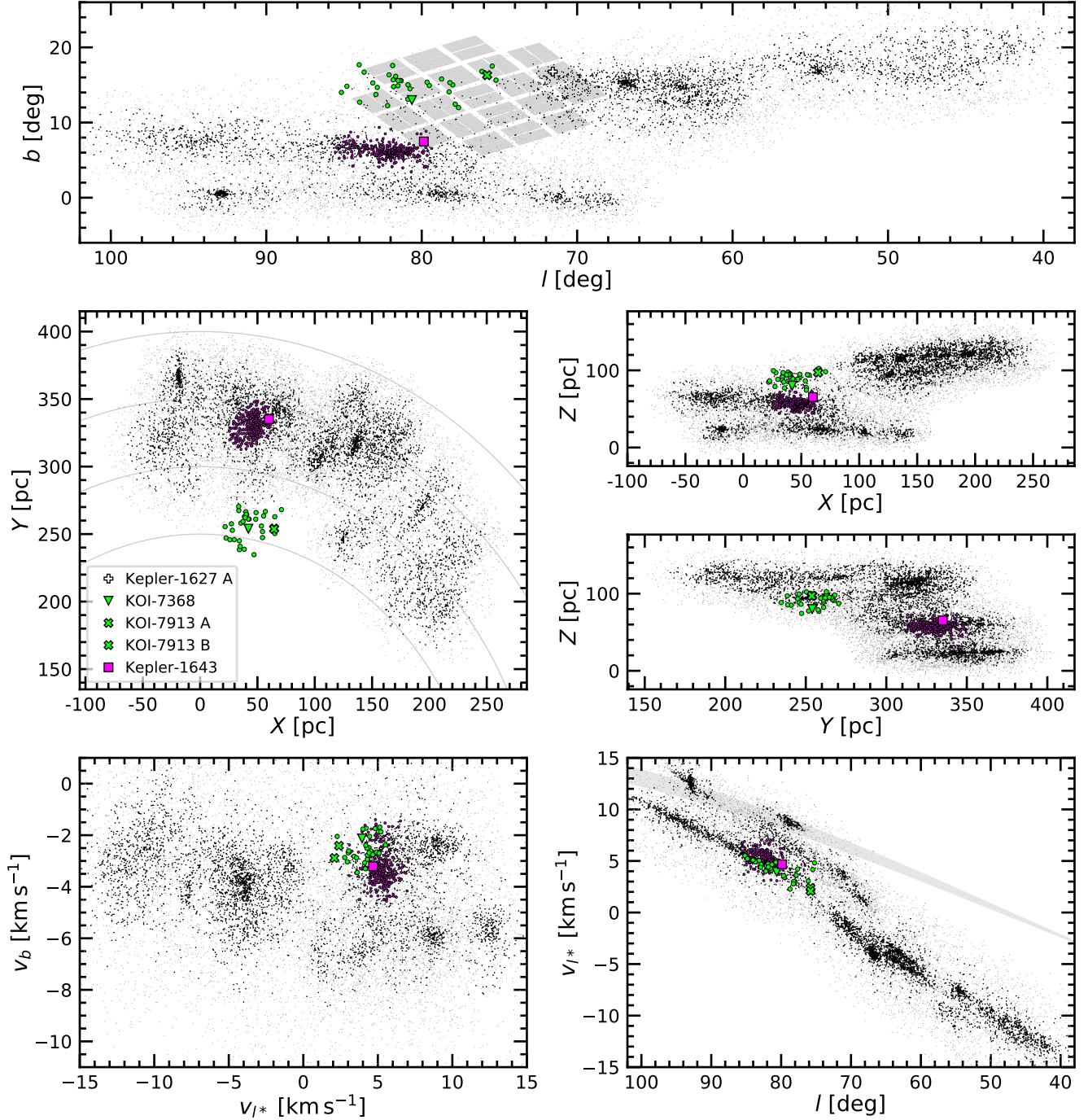
Figure 1. Positions and velocities of candidate members of the Cep-Her complex. *Top row*: On-sky positions in galactic coordinates. Black points are stars for which group membership is more secure than for gray points. Kepler-1627 is in the outskirts of the δ Lyr cluster (Bouma et al. 2022), which is centered at $\{l, b\} \approx \{66°, 12°\}$. *Middle row*: Galactic positions. The Sun is at $\{X, Y, Z\} = \{0, 0, 20.8\}$ pc; lines of constant heliocentric distance are shown between 250 and 400 pc, spaced by 50 pc. *Bottom row*: Galactic tangential velocities (left) and galactic longitudinal velocity versus galactic longitude (right). The gray band in the lower-right shows the ± 1-σ projection of the Solar velocity with respect to the local standard of rest. There is a strong spatial and kinematic overlap between Kepler-1643 and RSG-5 (magenta). The local population of candidate young stars around KOI-7368 and KOI-7913 is more diffuse – we call this region "CH-2" (lime-green). The selection method for the black, gray, purple, and green points is described in Section 2.2.

long contraction timescales, or massive stars near the zero-age main sequence due to their rapid evolutionary timescales.

The second step is to perform an unsupervised HDB-Scan clustering on the photometrically selected population (Campello et al. 2015; McInnes et al. 2017). The parameters we use in this clustering analysis are $\{X, Y, Z, cv_b, cv_{l*}\}$, where c is the size-velocity corrective factor, which is taken as $c = 6\,\mathrm{pc/km\,s^{-1}}$ to ensure that the spatial and velocity scales have identical standard deviations. Positions are computed assuming the `astropy v4.0` coordinate standard (Astropy Collaboration et al. 2018), which places the Sun 8122 pc from the galactic center, and assumes the solar velocity with respect to the local standard of rest from Schön-rich et al. (2010). As input parameters to HDBScan, we set the minimum ϵ threshold past which clusters cannot be fragmented as 25 pc in physical space, and c km s^{-1} in velocity. The minimum cluster size N is set to 10, as is k, the parameter used to define the "core distance" density metric.

This unsupervised clustering in our case yielded 8 distinct groups. These groups are then used as the "seed" populations for the third step, which is to search for objects at least as close to the 10$^{\text{th}}$ nearest HDBSCAN-identified member in space-velocity coordinates. This third step yields stars that are spatially and kinematically close to the photometrically-young stars, but which cannot be identified as young based on their positions in color versus absolute magnitude.

The outcome of the analysis up to the point of the third step is shown in Figure 1. To enable a selection cut that filters out field-star contaminants, we also compute a weight metric, defined such that the group member with the smallest core distance has a weight of 1, the group member with the greatest core distance has a weight of 0, and weights for the other group members are log-normally distributed between these two extremes. In Figure 1, we show 12,436 objects with weight exceeding 0.02 as gray points, and over-plot 4,763 objects with weights exceeding 0.10 as black points.[2] The previously known δ Lyr cluster ($l, b = 68°, 15°$; $v_{l'}, v_b = -4.5\,\mathrm{km\,s^{-1}}, -4\,\mathrm{km\,s^{-1}}$) is visible, as is RSG-5 ($l, b = 83°, 6°$; $v_{l'}, v_b = 5.5\,\mathrm{km\,s^{-1}}, -3.5\,\mathrm{km\,s^{-1}}$). Most of the other subclusters, including in Cep-Cyg ($l, b = 90°, 7°$) and Cerberus ($l, b = 48°, 18°$) are too small or dispersed to have previously been analyzed in great detail.

The fourth and final step was to cross-match our candidate Cep-Her member list against all known Kepler Objects of Interest. We used the Cumulative KOI table from the NASA Exoplanet Archive from 27 March 2022, and also compared against the `q1_q17_dr25` table (Thompson et al. 2018). From the candidate members with weights exceeding 0.02,

[2] These counts only include objects with reliable astrometry and photometry: $\varpi/\sigma_\varpi > 5$; $G/\sigma_G > 50$; $G_{\mathrm{RP}}/\sigma_{G_{RP}} > 20$; $G_{\mathrm{BP}}/\sigma_{G_{BP}} > 20$.

this yielded yielded 25 matches, of which 11 were known false positives, 6 were designated "confirmed", and 8 were designated "candidates". Inspection of the Kepler data validation summaries and Robovetter classifications for these objects then showed whether they were potentially consistent with being $i)$ planets, and $ii) \lesssim 10^8$ years old, based on the presence of rotational modulation at the expected period and amplitude (*e.g.*, Rebull et al. 2020, Figure 9). Four objects remained after this inspection: Kepler-1627, Kepler-1643, KOI-7368, and KOI-7913.

Figure 1 shows the positions of the KOIs along various projections. Kepler-1643 is near the core RSG-5 population both spatially and kinematically. KOI-7368 and KOI-7913 are in a diffuse region $\approx 40\,\mathrm{pc}$ above RSG-5 in Z and $\approx 100\,\mathrm{pc}$ closer to the Sun in Y. In tangential galactic velocity space, there may be some kinematic overlap between the region the latter two KOIs are in, and the main RSG-5 group.

We define two sets of stars in the local vicinity of our objects of interest. For candidate RSG-5 members, we require:

$$X/\mathrm{pc} \in [45, 75]$$
$$Y/\mathrm{pc} \in [320, 350]$$
$$Z/\mathrm{pc} \in [40, 70]$$
$$v_b/\mathrm{km\,s^{-1}} \in [-4, -3]$$
$$v_{l*}/\mathrm{km\,s^{-1}} \in [4, 6]$$

For the diffuse stars near KOI-7368 and KOI-7913, we require

$$X/\mathrm{pc} \in [20, 70]$$
$$Y/\mathrm{pc} \in [230, 270]$$
$$Z/\mathrm{pc} \in [75, 105]$$
$$v_b/\mathrm{km\,s^{-1}} \in [-3.5, -1.5]$$
$$v_{l*}/\mathrm{km\,s^{-1}} \in [2, 6]$$

and we call this latter set of stars "CH-2". These cuts yield 141 candidate RSG-5 members, and 37 candidate CH-2 members. An important consideration, especially for CH-2, is the contamination rate by field stars. We assess this in the following section.

2.3. *The Cluster's Age*

2.3.1. *Color-Absolute Magnitude Diagram*

Color-absolute magnitude diagrams (CAMDs) of the candidate RSG-5 and CH-2 members are shown in the upper row of Figure 2. The stars from the δ Lyr cluster are from Bouma et al. (2022), and the field stars are from the Gaia EDR3 Catalog of Nearby Stars (Gaia Collaboration et al. 2021b). To make these diagrams, we imposed the data filtering criteria from Gaia Collaboration et al. (2018a, Appendix B), which are designed to include binaries while omitting instrumental
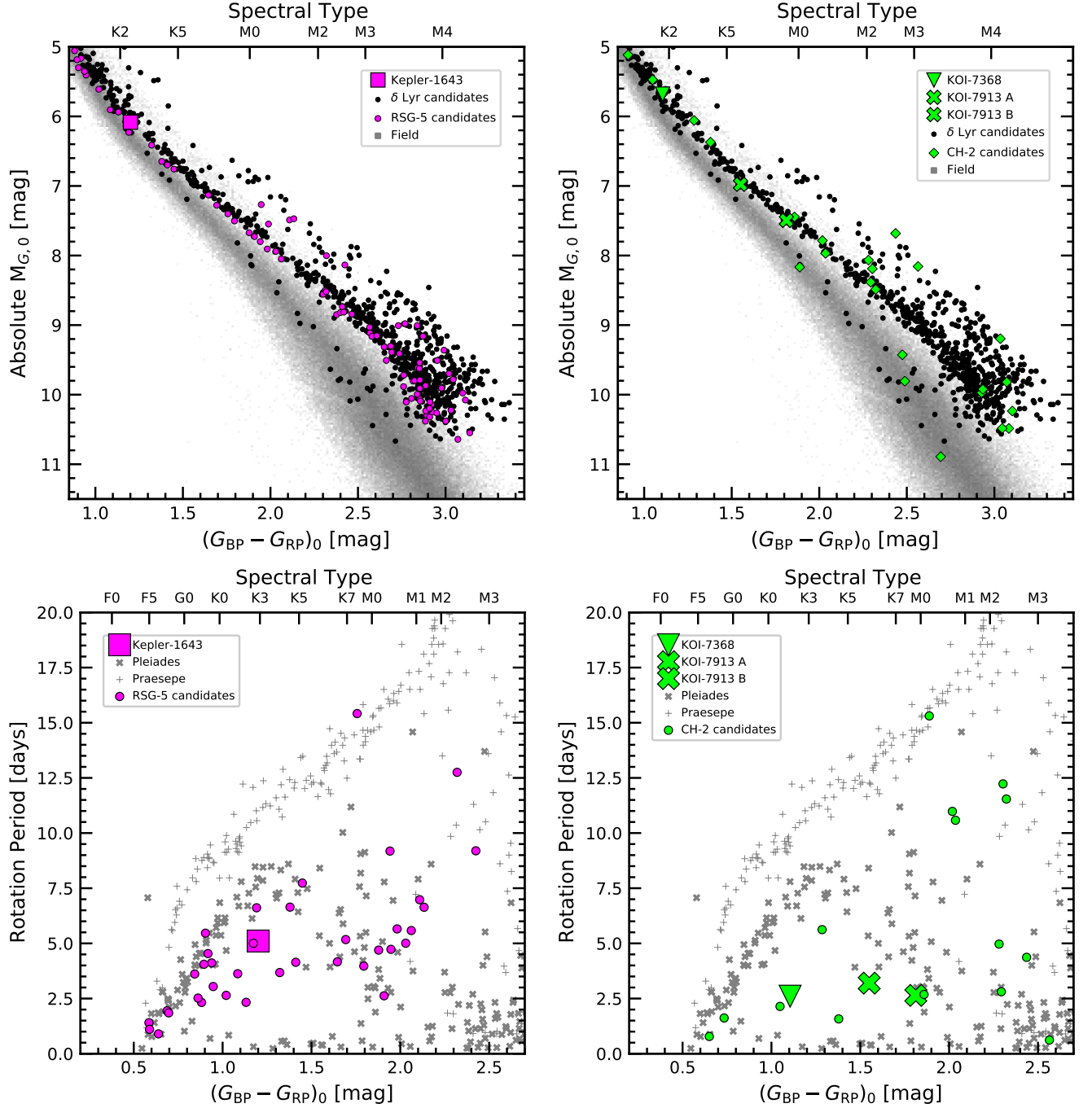
Figure 2. The stellar groups near KOI-7368, KOI-7913, and Kepler-1643 are 40 to 50 million years old. *Top row*: Color-absolute magnitude diagram of candidate Cep-Her members, in addition to candidate members of the δ Lyr cluster (≈ 38 Myr; Bouma et al. 2022) and and the Gaia EDR3 Catalog of Nearby Stars (gray background). The left and right columns shows stars in RSG-5 and CH-2, respectively. The range of colors is truncated to emphasize the pre-main-sequence. *Bottom row*: TESS and ZTF-derived stellar rotation periods, with the Pleiades (≈ 112 Myr) and Praesepe (≈ 650 Myr) shown for reference (Rebull et al. 2016; Douglas et al. 2017). The detection efficiency for reliable rotation periods falls off beyond $(G_{BP} - G_{RP})_0 \gtrsim 2.6$.

artifacts from for instance low photometric signal to noise, or a small number of visibility periods. We then corrected for extinction using the Lallement et al. (2018)[3] dust maps and the extinction coefficients $k_X \equiv A_X/A_0$ from Gaia Collaboration et al. (2018a), assuming that $A_0 = 3.1E(B-V)$. This yielded a mean and standard deviation for the reddening of $E(B-V) = 0.036 \pm 0.002$ for RSG-5, and $E(B-V) = 0.017 \pm 0.001$ for CH-2. By way of comparison, in Bouma et al. (2022) the same query for the δ Lyr cluster yielded $E(B-V) = 0.032 \pm 0.006$. Finally, for the plots we set the $(G_{BP}-G_{RP})_0$ color range to best visualize the region of maximal age information content: the pre-main-sequence.

The CAMDs show that for RSG-5, our membership selection gives stars that photometrically seem to almost all be on a tight pre-main-sequence locus. This implies a false positive rate of a few percent, at most. By comparison, our control sample (the δ Lyr candidates) has a false positive rate of $\approx 12\%$, based on the number of stars that photometrically appear to be more consistent with the field population than the bulk cluster population. For CH-2, our membership selection gives 27 objects in the color range displayed, and 23 of them appear to be consistent with being on the pre-main-sequence. This implies a false positive rate of $\approx 15\%$.

In addition, Figure 2 shows that the candidate RSG-5 and CH-2 members overlap with the δ Lyr cluster, and are therefore roughly the same age. To quantify this, we use the empirical method introduced by Gagné et al. (2020, see their Section 6.3). This idea of the method is to fit the pre-main-sequence loci of a set of reference clusters, and to then model the locus of the target cluster as a linear combination of these reference cluster loci. For our reference clusters, we used UCL, IC 2602, and the Pleiades, from the memberships reported by Damiani et al. (2019) and Cantat-Gaudin et al. (2018) respectively. We adopted ages of 16 Myr for UCL (Pecaut & Mamajek 2016), 38 Myr for IC 2602[4], and 112 Myr for the Pleiades (Dahm 2015). These assumptions and the consequent processing steps taken to exclude field stars as well as photometric and astrometric binaries were identical to those described in Bouma et al. (2022). The mean and standard deviation of the resulting age posterior are 46^{+9}_{-7} Myr for RSG-5, and 36^{+10}_{-8} Myr for CH-2. For comparison, the this procedure yields an age for the δ Lyr cluster of 38^{+6}_{-5} Myr. The slightly older isochronal age of RSG-5 is expected given that its locus is slightly bluer and less luminous in the upper left panel of Figure 2 relative to the δ Lyr cluster.

2.3.2. *Stellar Rotation Periods*

An independent way to assess the age of the candidate cluster members is to measure their stellar rotation periods. This approach can be achieved using surveys such as TESS (Ricker et al. 2015) and the Zwicky Transient Facility (ZTF, Bellm et al. 2019), and it leverages a storied tradition of rotation period measurement for benchmark open clusters (see *e.g.*, Skumanich 1972; Curtis et al. 2020). The TESS data in our case are especially useful, since they provide 3 to 5 lunar months of photometry for all of our candidate CH-2 and RSG-5 members.

We selected stars suitable for gyrochronology by requiring $(G_{BP}-G_{RP})_0 \geq 0.5$ to focus on FGKM stars that experience magnetic braking. For TESS, we also restricted our sample to $G < 16$, to ensure the stars are bright enough to extract usable light curves from the full-frame images (FFIs). The magnitude cut corresponds to $(G_{BP}-G_{RP})_0 < 2.6$ ($\sim$M3V) at the relevant distances. These cuts gave 19 stars in CH-2 and 42 stars in RSG-5. We extracted light curves from the TESS images for these stars using the `unpopular` package (Hattori et al. 2021), and regressed them against systematics with its causal pixel model. We measured rotation periods using Lomb-Scargle periodograms and visually vetted the results using an interactive program that allows us to switch between TESS Cycles, select particular sectors, flag stars with multiple periods, and correct half-period harmonics. For ZTF, we used the same color cut to focus on FGKM stars, but restricted the sample to $13 < G < 18$ to avoid the saturation limit on the bright end and ensure sufficient photometric precision at the faint end. We followed the procedure outlined in Curtis et al. (2020): we downloaded $8' \times 8'$ image cutouts, ran aperture photometry for the target and neighboring stars identified with Gaia, and used them to define a systematics correction to refine the target light curves. **How many stars with periods from TESS? ZTF? Overlap? Consistency?**

The lower panels of Figure 2 show the results. In RSG-5, 36/42 stars have rotation periods faster than the Pleiades (86%). This numerator omits the two stars with periods > 12 days visible in the lower-left panel of Figure 2. The age interpretation for these latter stars, particularly the $\approx$M2.5 dwarf, is not obvious. Rebull et al. (2018) for instance have found numerous M-dwarfs with 10-12 day rotation periods at ages of USco (~ 8 Myr), and some may still exist at ages of LCC (~ 16 Myr; L. Rebull in preparation). Regardless, given that nearly no field star outliers seem to be present on the RSG-5 CAMD, the fact that we do not detect rotation periods for $\approx$14% of stars should perhaps be taken as an indication for the fraction of stars for rotation periods might not be detectable, due to *e.g.*, pole-on stars having lower amplitude starspot modulation.

For CH-2, 13/19 stars have rotation periods that are obviously faster than their counterparts in the Pleiades (68%). 4

stars, not included in the preceding numerator, are M-dwarfs with rotation periods between 10 and 12.5 days. The age interpretation for these M-dwarfs is, as just discussed, not obvious. Regardless, the ≈15% false positive rate determined from the CAMD seems consistent with our fraction of detected rotation periods, given that RSG-5 was also missing rotation period detections for ≈15% of its candidate members, which all seemed photometrically consistent with being part of a single pre-main-sequence locus.

It is challenging to convert these stellar rotation periods to a precise age estimate, since on the pre-main-sequence the stars are spinning up due to thermal contraction rather than down due to magnetized braking. Regardless, the rotation period distributions of both CH-2 and RSG-5 seem consistent with other 30 Myr to 50 Myr clusters (*e.g.*, IC 2602 and IC 2391; Douglas et al. 2021). They also seem consistent with the false positive rate estimates determined from the color-absolute magnitude diagrams.

3. THE STARS

Some salient stellar parameters of the KOIs in Cep-Her can be gleaned by inspecting Figure 2. They span spectral types of G8V (Kepler-1627) to K8V (KOI-7913 A). The secondary in the KOI-7913 system is only marginally cooler than the primary. And since a Solar-mass star with solar metallicity arrives at the zero-age main sequence at $t \approx 40$ million years (Choi et al. 2016), these stars are all in the late stages of their pre-main-sequence contraction. Their heliocentric distances are ≈260 pc (KOI-7913 and KOI-7368, in CH-2) and ≈340 pc (Kepler-1643, in RSG-5).

The adopted stellar parameters are listed in Table 1. The stellar surface gravity, radius, mass, and density are found by interpolating against the MIST isochrones (Choi et al. 2016). The statistical uncertainties from this technique mostly originate from the parallax uncertaintes; the systematic uncertainties are taken to be the absolute difference between the PARSEC (Bressan et al. 2012) and MIST isochrones. Reported uncertainties are a quadrature sum of the statistical and systematic components.

To verify these parameters and to also analyze spectroscopic youth proxies such as the Li I 6708 Å doublet and Hα, we acquired spectra. We also acquired high resolution imaging for each system, to constrain the existence of visual companions, including possible bound binaries. The system-by-system details follow, and the the relevant results are also summarized in Table 1.

3.1. *Kepler 1643*

Spectra—For Kepler-1643, we acquired two iodine-free spectra from Keck/HIRES on the nights of 2020 August 16 and 2021 October 25. The acquisition and analysis followed the standard reduction techniques of the California

Table 1. Selected system parameters of Kepler-1643, KOI-7368, and KOI-7913.

Parameter	Value	Uncertainty	Comment
Kepler-1643			
Stellar parameters:			
Gaia G [mag]	13.836	±0.003	A
$T_{\rm eff}$ [K]	4916	±110	B
$\log g_\star$ [cgs]	4.502	±0.035	C
$R_\star$ [R$_\odot$]	0.855	±0.044	C
$M_\star$ [M$_\odot$]	0.845	±0.025	C
$\rho_\star$ [g cm^{-3}]	1.910	±0.271	C
$P_{\rm rot}$ [days]	5.106	±0.044	D
Li EW [mÅ]	126	+8, −4	E
Transit parameters:			
P [days]	5.3426258	±0.0000101	D
$R_{\rm p}/R_\star$	0.025	±0.001	D
b	0.58	±0.05	D
$R_{\rm p}$ [R$_\oplus$]	2.32	±0.14	D
t_{14} [hours]	2.409	±0.061	D
KOI-7368			
Stellar parameters:			
Gaia G [mag]	12.831	±0.004	A
$T_{\rm eff}$ [K]	5241	±50	F
$\log g_\star$ [cgs]	4.499	±0.030	C
$R_\star$ [R$_\odot$]	0.876	±0.035	C
$M_\star$ [M$_\odot$]	0.879	±0.018	C
$\rho_\star$ [g cm^{-3}]	1.840	±0.225	C
$P_{\rm rot}$ [days]	2.606	±0.038	D
Li EW [mÅ]	X	X	E
Transit parameters:			
P [days]	6.8430341	±0.0000125	D
$R_{\rm p}/R_\star$	0.023	±0.01	D
b	0.50	±0.06	D
$R_{\rm p}$ [R$_\oplus$]	2.22	±0.12	D
t_{14} [hours]	2.792	±0.075	D
KOI-7913 A			
Stellar parameters:			
Gaia G [mag]	14.200	±0.003	A
$T_{\rm eff}$ [K]	4324	±70	B
$\log g_\star$ [cgs]	4.523	±0.043	C
$R_\star$ [R$_\odot$]	0.790	±0.049	C
$M_\star$ [M$_\odot$]	0.760	±0.025	C
$\rho_\star$ [g cm^{-3}]	2.172	±0.379	C
$P_{\rm rot}$ [days]	3.387	±0.016	D
Li EW [mÅ]	X	X	E
$\Delta G_{\rm AB}$ [mag]	0.51	±0.01	F
Apparent sep. [au]	959.4	±1.9	F
Transit parameters:			
P [days]	24.2785706	±0.0002630	D
$R_{\rm p}/R_\star$	0.027	±0.001	D
b	0.30	±0.15	D
$R_{\rm p}$ [R$_\oplus$]	2.34	±0.18	D
t_{14} [hours]	4.396	0.207	D

NOTE— (A) Gaia Collaboration et al. (2021a). (B) HIRES SpecMatch-Emp (Yee et al. 2017). (C) Cluster isochrone (Choi et al. 2016; Bressan et al. 2012). (D) Kepler light curve. The full set of transit parameters are given in Appendix B. (E) HIRES (Bouma et al. 2021). (F) TRES SPC (Buchhave et al. 2010; Bieryla et al. 2021). (G) Magnitude difference and physical distance between primary and secondary; from Gaia EDR3. (H) HIRES SpecMatch-Synth (Petigura et al. 2017).

Planet Survey (Howard et al. 2010). We derived the stellar parameters ($T_{\rm eff}, \log g, R_\star$) using `SpecMatch-Emp` (Yee et al. 2017), which yielded values in < 1-σ agreement with those from the cluster-isochrone approach. This approach also yielded [Fe/H] $= 0.13 \pm 0.09$. Using the broadened synthetic templates from `SpecMatch-Synth` (Petigura et al. 2017), we found $v \sin i = 9.3 \pm 1.0\,{\rm km\,s^{-1}}$. The systemic radial velocity at the two sequence epochs was $-9.1 \pm 1.9\,{\rm km\,s^{-1}}$ and $-7.8 \pm 1.2\,{\rm km\,s^{-1}}$ respectively. To infer the equivalent width of the Li I 6708 Å doublet, we followed the procedure described by Bouma et al. (2021). This yielded a strong detection: $EW_{\rm Li} = 126^{+8}_{-4}$ mÅ, with values consistent at < 1-σ between the two epochs. The quoted value does not correct for the Fe I blend at 6707.44Å.

High-Resolution Imaging —We acquired adaptive optics imaging of Kepler-1643 on the night of 2019 June 28 using the NIRC2 imager on Keck-II (PI: E. Petigura). Using the narrow camera (FOV = 10.2″), we obtained 4 images in the K' filter ($\lambda = 2.12\,\mu$m) with a total exposure time of 320 s. We analyzed these data following Kraus et al. (2016), and determined the detection limits to visual companions by analyzing the residuals after subtracting an empirical PSF template. This procedure yielded contrast limits of $\Delta K' = 4.1$ mag at $\rho = 150$ mas, $\Delta K' = 5.8$ mag at $\rho = 300$ mas, and $\Delta K' = 8.3$ mag at $\rho > 1000$ mas.

3.2. *KOI-7368*

Spectra —For KOI-7368, we acquired a spectrum on 2015 June 1 using the echelle spectrograph (TRES; Fűrész et al. 2008) mounted at the Tillinghast 1.5m at the Fred Lawrence Whipple Observatory on Mt. Hopkins, AZ. The stellar parameter classification pipeline for the TRES spectra has been described by Bieryla et al. (2021). It is based on the synthetic template library originally constructed by Buchhave et al. (2010). The resulting stellar parameters ($T_{\rm eff}, \log g, R_\star$) agreed with those from the cluster-isochrone method within 1-σ, though the effective temperature is more precise by a factor of three. Auxiliary spectroscopic parameters included the metallicity [Fe/H] $= -0.02 \pm 0.08$, the equatorial velocity $v \sin i = 20.21 \pm 0.50\,{\rm km\,s^{-1}}$, and the systemic velocity $RV_{\rm sys} = -10.9 \pm 0.2\,{\rm km\,s^{-1}}$. The Li 6708Å EW measurement procedure yielded $EW_{\rm Li} = 236^{+16}_{-14}$ mÅ.

High-Resolution Imaging —We acquired adaptive optics imaging of KOI-7368 on the night of 2019 June 12 using the NIRC2 imager on Keck-II (PI: D. Huber). The observational configuration and reduction was identical as for Kepler-1643. No companions were detected, and the analysis of the image residuals yielded contrast limits of $\Delta K' = 5.2$ mag at $\rho = 150$ mas, $\Delta K' = 6.7$ mag at $\rho = 300$ mas, and $\Delta K' = 8.7$ mag at $\rho > 1000$ mas.

3.3. *KOI-7913*

Binarity —KOI-7913 is almost certainly a binary.[5] The northwest primary is ≈ 0.5 magnitudes brighter than the southeast secondary in optical passbands. The two stars are separated in Gaia EDR3 by 3″54 on-sky, and have parallaxes consistent within 1-σ (with an average $\varpi = 3.66 \pm 0.01$ mas). This corresponds to an apparent on-sky separation of 959 ± 2 au. Gaia EDR3 quotes $(\mu_{\alpha'}, \mu_\delta) = (2.439 \pm 0.015, 1.009 \pm 0.016)\,{\rm mas\,yr^{-1}}$ for the primary, and $(\mu_{\alpha'}, \mu_\delta) = (2.696 \pm 0.020, 0.650 \pm 0.021)\,{\rm mas\,yr^{-1}}$ for the secondary. Since two stars were resolved in the Kepler Input Catalog and are roughly one Kepler pixel apart, an accurate crowding metric has already been applied in the NASA Ames data products to correct the mean flux level (Morris et al. 2017). This is important for deriving accurate transit depths.

Spectra —We acquired Keck/HIRES spectra for KOI-7913 A on the night of 2021 Nov 13, and KOI-7913 B on the night of 2021 Oct 26. The usual `SpecMatch-Emp` (Yee et al. 2017) machinery yielded $T_{\rm eff,A} = 4324 \pm 70$ K, $T_{\rm eff,B} = 4038 \pm 70$ K. The remaining parameters were in agreement with those from the cluster isochrone. For the primary, we also found [Fe/H] $= -0.06 \pm 0.09$, $v \sin i = 13.3 \pm 1.0\,{\rm km\,s^{-1}}$, and $RV_{\rm sys} = -17.8 \pm 1.1\,{\rm km\,s^{-1}}$. These same parameters for the secondary were [Fe/H] $= -0.01 \pm 0.09$, $v \sin i = 10.7 \pm 1.0\,{\rm km\,s^{-1}}$, and $RV_{\rm sys} = -18.8 \pm 1.1\,{\rm km\,s^{-1}}$.

Regarding indicators of youth, the primary has a spectral type $\approx$K6V, while the secondary is $\approx$M0V. At ≈ 40 Myr, lithium 6708 Å absorption is not expected for the secondary, but might be present in the primary (*e.g.*, Soderblom et al. 2014, Figure 8). Conversely, Hα is expected to be in emission for for all M-dwarfs younger than ≈ 150 Myr (Kiman et al. 2021). At $\approx$M0V, if the secondary were in older than ≈ 500 Myr, it would be more common for its Hα component to be observed in absorption (Kiman et al. 2021, Figure 4). Hα emission in late K-dwarfs is rarer still. Based on the data from K. Rocio et al's analysis[6], a $\approx$K6V star should be emitting in Hα at 40 Myr, but not typically past ≈ 200 Myr. This presents a fairly direct test for the star's age.

Turning to the actual data, we find **X for lithium**. For Hα, **we see Y**.

High-Resolution Imaging —We acquired adaptive optics imaging of KOI-7913 on the night of 2020 Aug 27 using the NIRC2 imager on Keck-II (PI: D. Huber). The observational configuration and reduction was identical as before. The images showed KOI-7913 A, KOI-7913 B, and an additional faint star $\approx 0″99$ due East of KOI-7913 B. Applying the PSF-

[5] Relevant identifiers for the primary are KIC 8873450 = Gaia DR2/EDR3 2106235301785454208. For the secondary, they are KIC 8873448 = Gaia DR2/EDR3 2106235301785453824.

[6] Available at https://zenodo.org/record/4659293#.YkuKh27MKDV

fitting routines from Kraus et al. (2016), the tertiary star has a separation $\rho = 4397 \pm 3$ mas from the primary, at a position angle $231.17° \pm 0.02°$, with a $\Delta K' = 6.97 \pm 0.04$. While it is too faint to affect the interpretation of the KOI itself, it would be amusing if the faint neighbor were also comoving and young – at the age of the system, it would have a mass roughly between 10 and 15 $M_{\rm Jup}$. Additional imaging epochs will be required to tell.

4. THE PLANETS

4.1. *Kepler Data*

The Kepler space telescope observed Kepler-1643, KOI-7913, and KOI-7368 at a 30-minute cadence between May 2009 and April 2013. For all three systems quarters 1 through 17 were observed without any data gaps other than the usual quarterly roll. The top panel of Figure 3 shows a 50-day slice of the PDCSAP light curves for the three new Cep-Her candidates, along with Kepler-1627. In PDCSAP, nonastrophysical variability is removed through a cotrending approach that uses a set of basis vectors derived using singular value decomposition of a set of systematics-dominated stellar light curves (Smith et al. 2017). In our analysis, we used the PDCSAP light curves with the default optimal aperture (Smith et al. 2016). Cadences with non-zero quality flags were omitted. In all cases, the stars are dominated by spot-induced modulation with peak-to-peak variability between 2% and 10%. These signals are much larger than the transits, which have depth $\approx 0.1\%$. To quantify the stellar rotation periods, we calculated the Lomb-Scargle periodogram for each Kepler quarter independently. The resulting means and standard deviations are quoted in Table 1.

4.2. *Transit and Stellar Variability Model*

Our goals in fitting the Kepler light curves are twofold. First, we want to derive accurate planetary sizes and orbital properties. Second, we want to remove the stellar variability signal to enable a statistical assessment of the probability that the transit signals are planetary.

Our adopted approach was as follows. Given an initial guess for the transit ephemeris from the q1_q17_dr25 analysis (Thompson et al. 2018), the light curve was first trimmed to a local window around each transit of duration $\pm 3 \times t_{14}$. The local out-of-transit points were then fitted with a fourth-order polynomial, which was then divided out from the light curve. The resulting flattened transits were then fitted with a planetary transit under the assumption of quadratic limb darkening. Our model therefore included 8 free parameters for the transit ($\{P, t_0, \log R_{\rm p}/R_\star, b, u_1, u_2, R_\star, \log g\}$), 2 free parameters for the light curve normalization and a white noise jitter ($\{\langle f \rangle, \sigma_f\}$), and an additional 5 implicit parameters per transit through the polynomial.

We fitted the models using exoplanet (Foreman-Mackey et al. 2020). We assumed a Gaussian likelihood, and sampled using PyMC3's No-U-Turn Sampler (Hoffman & Gelman 2014), after having initialized using the maximum *a posteriori* (MAP) model. We used the Gelman & Rubin (1992) statistic ($\hat{R}$) as our convergence diagnostic. The results are shown in the lower panels of Figure 3, and the important derived parameters are in Table 1. The set of full parameters with their priors are given in Appendix B.

One weakness of our fitting approach is that we have fixed 5 implicit parameters per individual transit to their MAP values to remove the stellar variability signal. An alternative could be to fit the planetary transits simultaneously with the starspot-induced variability using, say, a quasiperiodic Gaussian process (GP). We explored this approach, but found that it required careful fine-tuning of the hyperparameter priors, otherwise the GP would tend to incorporate any variability that was not part of the transit, even if it was short-term variability attributable to flares, or simply instrumental noise. This failure mode is somewhat pernicious, in that it yields an ill-founded sense of confidence in an "overly clean" transit model fit. Although our model is simpler, it has the benefit that the white noise jitter never trades off with any parameter equivalent to a damping timescale for the coherence of the GP. It is also computationally efficient, and it captures the planetary parameters that we actually care about.

4.3. *Planet Validation*

In the future, it may be possible to obtain independent evidence for the Cep-Her planets to directly confirm their planetary nature. The most likely path would be through transit observations using a high-resolution spectrograph (see Bouma et al. 2022). In the interim, it is of interest whether the transit signals could be astrophysical false positives, or whether they can be argued to be planetary on a statistical basis. We adopt the Bayesian framework implemented in VESPA for this purpose (Morton 2012, 2015). Briefly summarized, the priors in VESPA take as given the binary star occurrence rate from Raghavan et al. (2010), direction-specific star counts from Girardi et al. (2005), and planet occurrence rates as described by Morton (2012, Section 3.4). The likelihoods are then evaluated by forward-modeling a synthetic population of eclipsing bodies for each possible astrophysical model class, in which each population member has a particular trapezoidal eclipse depth, total duration, and ingress duration. These summary statistics are then compared against the actual photometric data to evaluate the probabilities of false positive scenarios such as foreground eclipsing binaries, hierarchical eclipsing binaries, and background eclipsing binaries.

Kepler-1643—Kepler-1643 b (KOI-6186.01) was already validated as a transiting planet by Morton et al. (2016). Based on the Q1-Q17 DR25 False Positive Probability table hosted
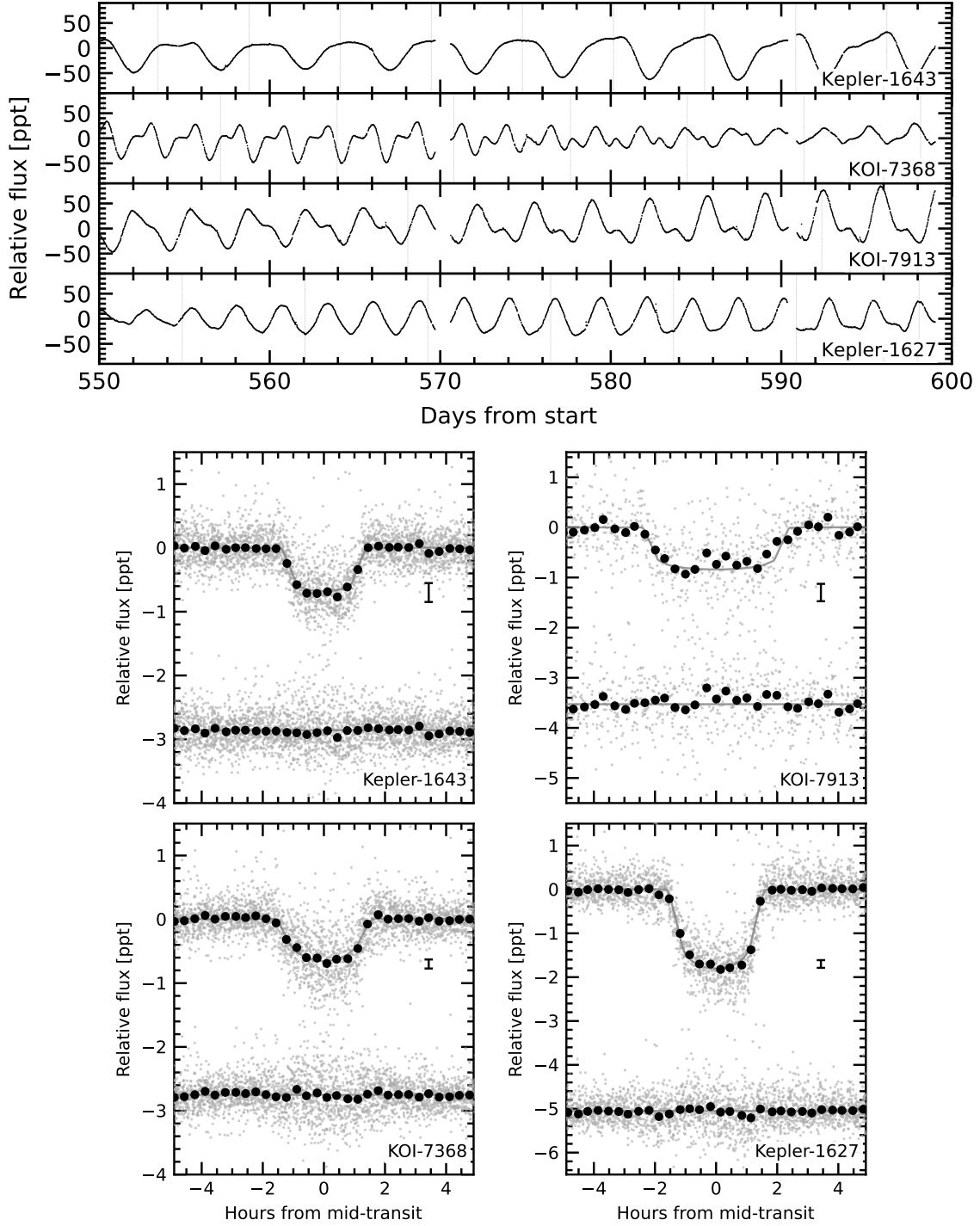
Figure 3. Raw and processed light curves for the Kepler Objects of Interest in Cep-Her. *Top*: 50 day light curve segment from the 3.9 years of Kepler data. The ordinate shows the `PDCSAP` median-subtracted flux in units of parts-per-thousand ($\times 10^{-3}$). The dominant signal is induced by starspots. *Bottom*: Phase-folded transits of Kepler-1643, KOI-7913, KOI-7368, and Kepler-1627 with stellar variability removed. The maximum *a posteriori* transit model is shown with the gray line, and the residual after subtracting the transit model is vertially displaced. Windows over 10 hours are shown. Gray points are individual flux measurements; black points are binned to 20 minute intervals, and have a representative 1-σ error bar in the center-right of each panel.

at the NASA Exoplanet Archive, they found a probability for any of the considered false positive scenarios of 9×10^{-6}. Repeating the calculation with our own stellar-variability correction and the new NIRC2 imaging constraints, we find FPP = 6×10^{-9}, where the improvement is presumably due to the new NIRC2 contrast curves. Figure 3 shows the intuitive justification for the strong statistical result: the transit is flat and has a reasonably high S/N (≈ 47), which is difficult to reproduce with eclipsing binary models.

An interesting aside on Kepler-1643 is that it formally failed the centroid shift test in the `q1_q17_dr25_koi` data release, with the angular distance between the target star position and the location of the transiting source being reported as $0''99$ (4.4-σ). This seems to be mostly due to two outlying quarters (Q2 and Q6) driving the offset – the centroid locations from the other Kepler quarters are all consistent within $\lesssim 0''5$. Nonetheless, this is an instructive exercise in how variable stars can complicate centroid-based vetting tests. The centroid shifts measured by these tests are determined from the in- and out-of-transit flux-weighted centroids, but for our stars there is no static baseline in either in- or out-of-transit phase.

KOI-7368 —KOI-7368.01 is listed on the NASA Exoplanet Archive as a "CANDIDATE" planet. The Q1-Q17 DR25 False Positive Probability table however lists its probability of being an astrophysical false positive as "1.0". However, given that none of the other columns in this table are populated, this is likely a database entry error (**ask Jessie**). Performing the validation calculation using our new NIRC2 imaging constraints, we find FPP $\approx 4 \times 10^{-3}$. While not as convincing as Kepler-1643, this formally clears the usual threshold for calling the planet statistically validated (Morton 2012). The S/N of the transit itself is ≈ 32, which indicates that it is unlikely to be caused by systematic noise in the light curve. Visually, one can also inspect each individual transit window in the light curve itself. This exercise shows a weak notch in each case; over the 198 observed transits, the resulting signal seems sensible.

Why was KOI-7368 not previously validated? One reason could be the high stellar variability. Another reason could be that it also formally fails the centroid shift test, similar to Kepler-1643. In the case of KOI-7368, the reported offset is marginally less significant ($0''22$; 3.0-σ). Again, inspection of the data validation reports shows that this is caused by a few outlying quarters: in this case Q4, Q5, Q8, and Q12. The fact that the remaining quarters show a more consistent scatter suggests that these outliers are again caused by stellar variability local to the transits, rather than by an astrophysical offset. Our imaging also shows that there are no neighboring sources that could cause an offset of the observed amplitude.

KOI-7913 —KOI-7913.01 is listed on the NASA Exoplanet Archive as a "CANDIDATE" planet. The Q1-Q17 DR25 False Positive Probability table lists its probability of being an astrophysical false positive as 1.4×10^{-4}, with the most likely false positive scenario being a blended eclipsing binary. Repeating the calculation with our new detrending and contrast curves, we find a similar result: FPP = 1.3×10^{-4}. While the transit has the lowest S/N of any of the objects discusssed (S/N = 14), its lower FPP relative to KOI-7368 can be understood through its relatively flat-bottomed shape, combined with its long transit duration relative to plausible eclipsing binary models (Figure 3).

The disposition of KOI-7913.01 has previously been debated: in `q1_q17_dr25_koi` the source was flagged as a "FALSE POSITIVE", with the comment "CENT_KIC_POS—HALO_GHOST". This comment and disposition seem to have been removed in the `q1_q17_dr25_sup_koi` data release, which renamed it a "CANDIDATE", without any flag given. As described by Thompson et al. (2018), the "CENT_KIC_POS" flag is an indication that the measured source centroid is offset from its expected location in the Kepler Input Catalog. The final Data Validation Reports, generated 2016 Jan 30, do not seem to show this. Moreover, the statistical significance of any centroid offset seems to be lower than for KOI-7368 and Kepler-1643 (which, as we have argued, both show centroid offsets that seem to be explained by the stellar variability).

What of the "HALO_GHOST" flag? This test measures the transit strength for the pixels inside the aperture, and compares it to that measured in the ring of pixels around said aperture (the "halo"). Generally one expects the transit signal to be strongest in the central aperture, rather than the halo. Two types of false positive scenarios can change this and trigger the flag: the first is when optical ghosts from bright eclipsing binaries reflect off the CCD, and contaminate the target star. The second is when the PRF of nearby stars directly overlaps with the PRF of the target star (see Thompson et al. 2018, Section A.5.2).

The most obvious explanation for KOI-7913 is the latter case, since KOI-7913 B is ≈ 0.9 Kepler pixels away from Kepler-7913 A. Due to the on-sky orientation of KOI-7913 A and KOI-7913 B, the default "optimal aperture" selected in Q3, Q7, Q11, and Q15 in fact included both stars, while for the remaining quarters KOI-7913 B was (correctly) excluded from the optimal aperture (see pages 35 through 71 of the Data Validation Report.)

As a test, we opted to re-extract the light curves from the target pixel files for these particular cases. **Comparing the pixels on-target, and found We found...**

5. DISCUSSION & CONCLUSION
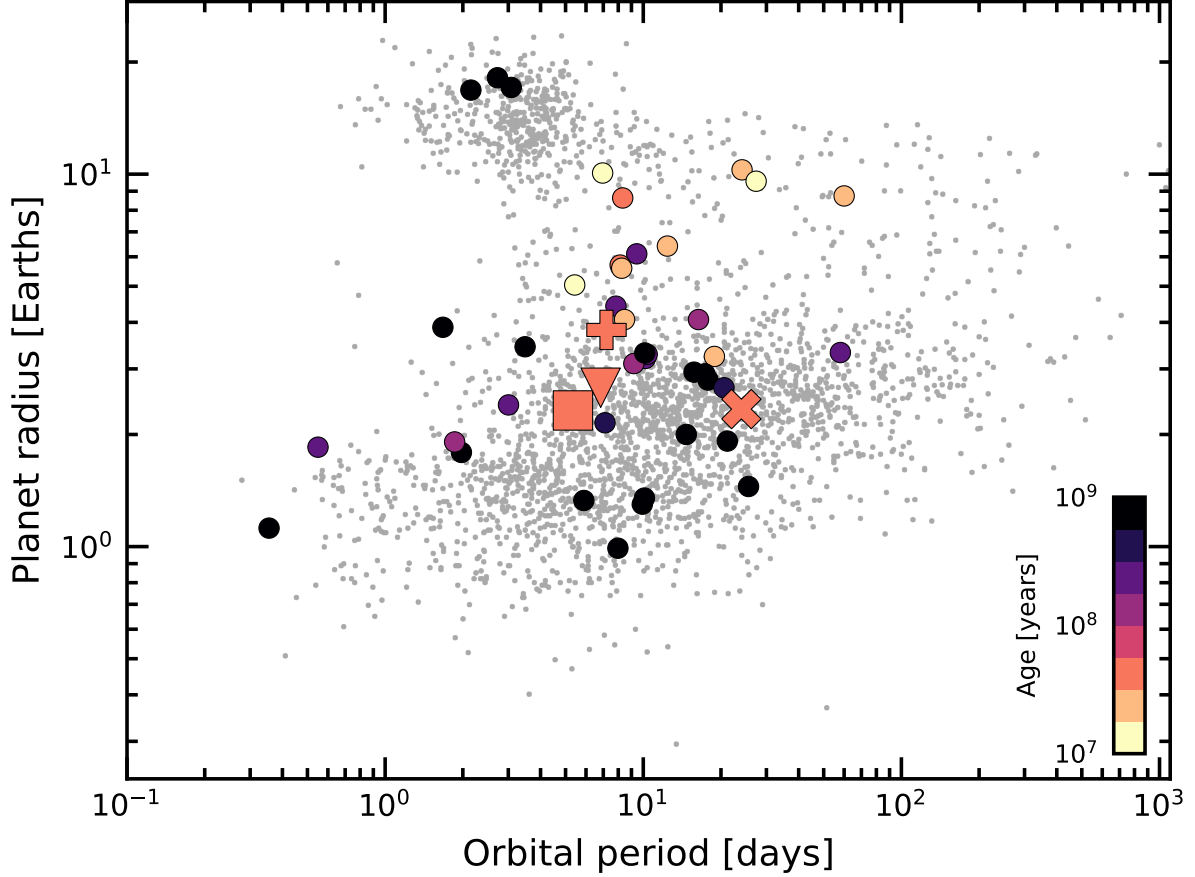
5.1. *Is CH-2 really a star cluster?*

Figure 4. Radii, orbital periods, and ages of transiting exoplanets. Planets younger than a gigayear with $\tau/\sigma_\tau > 3$ are emphasized, where τ is the age and σ_τ is its uncertainty. Kepler-1627 (+), KOI-7368 (down-triangle), KOI-7913 (X), Kepler-1643 (diamond). The large sizes of the youngest transiting planets could be tied to a selection effect. Kepler-1643, KOI-7368, and KOI-7913 have normal mini-Neptune sizes of 2 to $3\,R_\oplus$, which is a novelty given their ages. Parameters are from the NASA Exoplanet Archive (2022 Apr 5).

RSG-5, and Kepler-1643's membership inside it, clearly meet the typical expectations of a star claimed to be in an open cluster. RSG-5 shows an obvious overdensity relative to the local field population (*e.g.*, Figure 1), and our membership selection easily produces a clean pre-main-sequence locus in color-absolute magnitude space (Figure 2). CH-2, and KOI-7913 and KOI-7368's membership inside it, do not meet those expectations in as obvious a manner. This is because this association of stars is diffuse.

To quantify the density discrepancy, we can compare the spatial and velocity volumes searched to select candidate members of each cluster. For RSG-5, we drew 141 candidate members from a $30\,\mathrm{pc} \times 30\,\mathrm{pc} \times 30\,\mathrm{pc}$ spatial cube, given a $1\,\mathrm{km\,s^{-1}} \times 2\,\mathrm{km\,s^{-1}}$ rectangle in apparent galactic velocity. For CH-2, our 37 candidate members came from a spatial cube of dimension $50\,\mathrm{pc} \times 40\,\mathrm{pc} \times 30\,\mathrm{pc}$, and the velocity rectangle of $2\,\mathrm{km\,s^{-1}} \times 4\,\mathrm{km\,s^{-1}}$. If we define the "searched volume" in units of $\mathrm{pc}^3 (\mathrm{km\,s^{-1}})^2$, then the volume ratio of CH-2:RSG-5 is $\approx 9{:}1$. The density (number of stars per unit searched volume) within RSG-5 relative to CH-2 similarly comes out to 34 to 1.

So what makes a star cluster? Historic answers to this question have recently by reviewed by Krumholz et al. (2019): some definitions that have been offered include criteria such as being gravitationally bound, and having a mass density that significantly exceeds the mean in a cluster's galactic neighborhood. We prefer a modified version of the definition adopted by Krumholz et al. (2019): for our purposes a star cluster is a group of at least 12 stars that was physically associated at its time of formation. The somewhat arbitrary "12" is set to distinguish clusters from high-order multiple star systems. We therefore explicitly include dissolved clusters and their tidal tails in our concept of clusters. We also explicitly exclude the idea that a particular number of stars per unit spatial volume is required to define a cluster. The latter point acknowledges the fact that an important factor in cluster identification is now also the number per unit velocity volume, whether in 2-dimensional tangential velocity, or when including the third radial component. Perhaps once stellar rotation periods and chemical abundances reach the same level of ubiquity as stellar proper motions, they

might enable further refinement of our ability in cluster discovery.

From a data-driven perspective, how do we demonstrate that a star is in a cluster, *i.e.*, that it is part of a group of stars that was physically associated at its time of formation? Back-integrating the orbits is one convincing approach, but it does not always work **(CITE)**. The relatively minimal approach suggested by Tofflemire et al. (2021) is intriguing: search for coeval, phase-space neighbors, measure their ages, and determine if they share a common age. This approach is more accurately be described as a method for determining whether a star is currently associated with a set of coeval stars, which is much easier to determine than what the association looked like in the past. From this standard, our analysis thus far of CH-2 has already demonstrated the existence of such an assocation.

A crucial logical step in this method however is to ensure that the (automated) search process for coeval phase-space neighbors in fact produces neighbors at a rate different from what it would for field stars.

And so we ask: what is the density of field stars in the CH-2 region? If we had applied Ronan's pre-main-sequence selection, + HDBScan, + local neighbors... what would we have gotten? Similarly... if you just applied Adam Kraus' Comove What is the likelihood we are fooling ourselves?

5.2. *Normal-Sized Mini-Neptunes Exist at 40 Myr*

Current thinking about the origins and evolution of lose-in mini-Neptunes has recently been reviewed by Bean et al. (2021). In the context of the existing exoplanet population, the most significant novelty about Kepler-1643 b, KOI-7368.01, and KOI-7913 is that they have normal sizes. More specifically, the size distribution of mini-Neptunes spans $\approx 1.8\,R_\oplus$ to $\approx 3.6\,R_\oplus$, with a peak at $\approx 2.4\,R_\oplus$ (Fulton et al. 2017, Figure 7). Figure 4 shows the sizes, orbital periods, and ages of known transiting planets, emphasizing those with precise ages. Considering planets younger than 10^8 years, the smallest previously known were AU Mic c ($\approx 3.0 \pm 0.2\,R_\oplus$, averaging the results of Martioli et al. 2021 and Gilbert et al. 2022), Kepler-1627 Ab ($3.8 \pm 0.2\,R_\oplus$; Bouma et al. 2022), and AU Mic d ($4.2 \pm 0.2\,R_\oplus$; Plavchan et al. 2020). The other transiting planets younger than 10^8 years are much larger, with sizes between 4 and $10\,R_\oplus$ (Mann et al. 2016; David et al. 2016; Benatti et al. 2019; David et al. 2019; Newton et al. 2019; Rizzuto et al. 2020; Bouma et al. 2020).

Run some evolutionary models, make some comments about the core mass, KH timescale, etc.

5.3. *Summary*

We have argued that Kepler-1643 b, KOI-7368.01, and KOI-7913 *i)* are 40 to 50 million years old, and *ii)* that each signal is most likely planetary. The evidence for the planetary interpretation comes from an application of VESPA to the Kepler data, alongside new adaptive optics imaging from NIRC2. The validity of the VESPA framework rests on the premise that non-astrophysical false positives, including false alarms and known neighboring eclipsing binaries, can be rejected. Kepler-1643 and KOI-7368 both pass all but one of the canonical vetting checks: the check for centroid offsets between the in and out-of-transit phases. For both cases, we have argued the weak observed shifts are most likely caused by starspot-induced variability in specific quarters shifting the stellar center-of-light.

Each system has multiple indicators of youth that support the reported ages. For Kepler-1643, perhaps the strongest youth indicator is its physical and kinematic association with RSG-5. Based on the color-absolute magnitude diagram, we are able to select members of this cluster with a false positive rate of $\ll 5\%$ (Figure 2); Kepler-1643 is one such member. The stellar rotation period period agrees with this assessment, and **its lithium is a little low**.

The spatio-kinematic argument for the youth of KOI-7368 and KOI-7913 are weaker because they are in an association of stars, CH-2, that is more diffuse. For KOI-7913, stronger indicators of its age perhaps come from its binary. Both stellar components in KOI-7913 have isochronal ages consistent with 40 Myr, but the isochronal measurement for the secondary is more constraining since it is less massive. Both components also show Hα in emission, which for the $\approx$K6V primary is a good indicator that the star is $\lesssim 100$ Myr old. For KOI-7368, which is slightly more massive, the Li 6708Å EW measurement and stellar rotation period are more constraining, and provide independent verification of the star's youth.

14

Software: `astrobase` (Bhatti et al. 2018), `astropy` (Astropy Collaboration et al. 2018), `astroquery` (Ginsburg et al. 2018), `exoplanet` (Foreman-Mackey et al. 2020), and its dependencies (Agol et al. 2020; Kipping 2013; Luger et al. 2019; Theano Development Team 2016), `PyMC3` (Salvatier et al. 2016), `scipy` (Jones et al. 2001), `VESPA` (Morton 2012, 2015),

Facilities: *Astrometry*: Gaia (Gaia Collaboration et al. 2018b, 2021a). *Imaging*: Second Generation Digitized Sky Survey. Keck:II (NIRC2; www2.keck.hawaii.edu/inst/nirc2). *Spectroscopy*: Tillinghast:1.5m (TRES; Fűrész et al. 2008). Keck:I (HIRES; Vogt et al. 1994). *Photometry*: Kepler (Borucki et al. 2010), TESS (Ricker et al. 2015).

REFERENCES

Agol, E., Luger, R., & Foreman-Mackey, D. 2020, AJ, 159, 123

Arevalo, R. T., Tamayo, D., & Cranmer, M. 2022, arXiv:2203.02805 [astro-ph], arXiv: 2203.02805

Astropy Collaboration, Price-Whelan, A. M., Sipőcz, B. M., et al. 2018, AJ, 156, 123

Bean, J. L., Raymond, S. N., & Owen, J. E. 2021, Journal of Geophysical Research (Planets), 126, e06639

Bellm, E. C., Kulkarni, S. R., Graham, M. J., et al. 2019, PASP, 131, 018002

Benatti, S., Nardiello, D., Malavolta, L., et al. 2019, A&A, 630, A81

Bhatti, W., Bouma, L. G., & Wallace, J. 2018, astrobase, https://doi.org/10.5281/zenodo.1469822

Bieryla, A., Tronsgaard, R., Buchhave, L. A., et al. 2021, in Posters from the TESS Science Conference II (TSC2), 124

Borucki, W. J., Koch, D., Basri, G., et al. 2010, Science, 327, 977

Bossini, D., Vallenari, A., Bragaglia, A., et al. 2019, A&A, 623, A108

Bouma, L. G., Curtis, J. L., Hartman, J. D., Winn, J. N., & Bakos, G. A. 2021, arXiv:2107.08050 [astro-ph]

Bouma, L. G., Hartman, J. D., Brahm, R., et al. 2020, AJ, 160, 239

Bouma, L. G., Curtis, J. L., Masuda, K., et al. 2022, AJ, 163, 121

Bressan, A., Marigo, P., Girardi, L., et al. 2012, MNRAS, 427, 127

Buchhave, L. A., Bakos, G. A., Hartman, J. D., et al. 2010, ApJ, 720, 1118

Campello, R. J. G. B., Moulavi, D., Zimek, A., & Sander, J. 2015, ACM Transactions on Knowledge Discovery from Data, 10, 5:1

Cantat-Gaudin, T., Jordi, C., Vallenari, A., et al. 2018, A&A, 618, A93

Choi, J., Dotter, A., Conroy, C., et al. 2016, ApJ, 823, 102

Curtis, J. L., Agüeros, M. A., Mamajek, E. E., Wright, J. T., & Cummings, J. D. 2019, AJ, 158, 77

Curtis, J. L., Agüeros, M. A., Matt, S. P., et al. 2020, ApJ, 904, 140

Dahm, S. E. 2015, ApJ, 813, 108

Damiani, F., Prisinzano, L., Pillitteri, I., Micela, G., & Sciortino, S. 2019, A&A, 623, A112

David, T., Hillenbrand, L., & Petigura, E. 2016, Nature, 534, 658

David, T. J., & Hillenbrand, L. A. 2015, ApJ, 804, 146

David, T. J., Petigura, E. A., Luger, R., et al. 2019, ApJL, 885, L12

Dawson, R. I., & Johnson, J. A. 2018, ARA&A, 56, 175

Dinnbier, F., & Kroupa, P. 2020, a, 640, A85

Dobbie, P. D., Lodieu, N., & Sharp, R. G. 2010, MNRAS, 409, 1002

Douglas, S. T., Agüeros, M. A., Covey, K. R., & Kraus, A. 2017, ApJ, 842, 83

Douglas, S. T., Pérez Chávez, J., Cargile, P. A., et al. 2021, 10.5281/zenodo.5131306

Fűrész, G., Szentgyorgyi, A. H., & Meibom, S. 2008, 287

Foreman-Mackey, D., Czekala, I., Luger, R., et al. 2020, exoplanet-dev/exoplanet v0.2.6

Fulton, B. J., Petigura, E. A., Howard, A. W., et al. 2017, AJ, 154, 109

Gagné, J., David, T. J., Mamajek, E. E., et al. 2020, ApJ, 903, 96

Gagné, J., Faherty, J. K., Moranta, L., & Popinchalk, M. 2021, arXiv:2106.11873 [astro-ph], arXiv: 2106.11873

Gaia Collaboration, Babusiaux, C., van Leeuwen, F., et al. 2018a, A&A, 616, A10

Gaia Collaboration, Brown, A. G. A., Vallenari, A., et al. 2018b, A&A, 616, A1

—. 2021a, A&A, 649, A1

Gaia Collaboration, Smart, R. L., Sarro, L. M., et al. 2021b, A&A, 649, A6

Gelman, A., & Rubin, D. B. 1992, Statistical Science, 7, 457, publisher: Institute of Mathematical Statistics

Gilbert, E. A., Barclay, T., Quintana, E. V., et al. 2022, AJ, 163, 147

Ginsburg, A., Sipocz, B., Madhura Parikh, et al. 2018, Astropy/Astroquery: V0.3.7 Release

Ginzburg, S., Schlichting, H. E., & Sari, R. 2018, MNRAS, 476, 759

Girardi, L., Groenewegen, M. A. T., Hatziminaoglou, E., & da Costa, L. 2005, A&A, 436, 895

Goldberg, M., & Batygin, K. 2022, arXiv:2203.00801 [astro-ph], arXiv: 2203.00801

Hattori, S., Foreman-Mackey, D., Hogg, D. W., et al. 2021, arXiv e-prints, arXiv:2106.15063

Hawkins, K., Lucey, M., & Curtis, J. 2020, MNRAS, 496, 2422

Hedges, C., Hughes, A., Zhou, G., et al. 2021, AJ, 162, 54

Hoffman, M. D., & Gelman, A. 2014, Journal of Machine Learning Research, 15, 1593

Howard, A. W., Johnson, J. A., Marcy, G. W., et al. 2010, ApJ, 721, 1467

Jerabkova, T., Boffin, H. M. J., Beccari, G., et al. 2021, a, 647, A137

Jones, E., Oliphant, T., Peterson, P., et al. 2001, Open source scientific tools for Python

Kerr, R. M. P., Rizzuto, A. C., Kraus, A. L., & Offner, S. S. R. 2021, ApJ, 917, 23, aDS Bibcode: 2021ApJ...917...23K

Kiman, R., Faherty, J. K., Cruz, K. L., et al. 2021, AJ, 161, 277

Kipping, D. M. 2013, MNRAS, 435, 2152

Kounkel, M., & Covey, K. 2019, AJ, 158, 122

Kraus, A. L., Ireland, M. J., Huber, D., Mann, A. W., & Dupuy, T. J. 2016, AJ, 152, 8

Krumholz, M. R., McKee, C. F., & Bland-Hawthorn, J. 2019, ARA&A, 57, 227

Lallement, R., Babusiaux, C., Vergely, J. L., et al. 2019, a, 625, A135

Lallement, R., Capitanio, L., Ruiz-Dern, L., et al. 2018, A&A, 616, A132

Lee, E. J., & Connors, N. J. 2021, ApJ, 908, 32, aDS Bibcode: 2021ApJ...908...32L

Lopez, E. D., Fortney, J. J., & Miller, N. 2012, ApJ, 761, 59

Luger, R., Agol, E., Foreman-Mackey, D., et al. 2019, AJ, 157, 64

Mann, A. W., Newton, E. R., Rizzuto, A. C., et al. 2016, AJ, 152, 61

Mann, A. W., Gaidos, E., Vanderburg, A., et al. 2017, AJ, 153, 64

Martioli, E., Hébrard, G., Correia, A. C. M., Laskar, J., & Lecavelier des Etangs, A. 2021, A&A, 649, A177

McInnes, L., Healy, J., & Astels, S. 2017, The Journal of Open Source Software, 2, 205

Meingast, S., Alves, J., & Fürnkranz, V. 2019, A&A, 622, L13

Meingast, S., Alves, J., & Rottensteiner, A. 2021, A&A, 645, A84

Morris, R. L., Twicken, J. D., Smith, J. C., et al. 2017, Kepler Data Processing Handbook: Photometric Analysis, Kepler Science Document KSCI-19081-002

Morton, T. D. 2012, ApJ, 761, 6

Morton, T. D. 2015, VESPA: False positive probabilities calculator, Astrophysics Source Code Library, ascl:1503.011

Morton, T. D., Bryson, S. T., Coughlin, J. L., et al. 2016, ApJ, 822, 86

Nardiello, D., Piotto, G., Deleuil, M., et al. 2020, MNRAS, 495, 4924

Newton, E. R., Mann, A. W., Tofflemire, B. M., et al. 2019, ApJ, 880, L17

Owen, J. E., & Wu, Y. 2013, ApJ, 775, 105

Pecaut, M. J., & Mamajek, E. E. 2016, MNRAS, 461, 794

Petigura, E. A., Howard, A. W., Marcy, G. W., et al. 2017, AJ, 154, 107, aDS Bibcode: 2017AJ....154..107P

Plavchan, P., Barclay, T., Gagné, J., et al. 2020, Nature, 582, 497

Raghavan, D., McAlister, H. A., Henry, T. J., et al. 2010, ApJS, 190, 1

Randich, S., Tognelli, E., Jackson, R., et al. 2018, A&A, 612, A99

Rebull, L. M., Stauffer, J. R., Cody, A. M., et al. 2020

—. 2018, AJ, 155, 196

Rebull, L. M., Stauffer, J. R., Bouvier, J., et al. 2016, AJ, 152, 113

Ricker, G. R., Winn, J. N., Vanderspek, R., et al. 2015, JATIS, 1, 014003

Rizzuto, A. C., Newton, E. R., Mann, A. W., et al. 2020, AJ, 160, 33

Röser, S., Schilbach, E., & Goldman, B. 2016, a, 595, A22

Salvatier, J., Wieckiâ, T. V., & Fonnesbeck, C. 2016, PyMC3: Python probabilistic programming framework

Schönrich, R., Binney, J., & Dehnen, W. 2010, MNRAS, 403, 1829

Skumanich, A. 1972, ApJ, 171, 565

Smith, J. C., Morris, R. L., Jenkins, J. M., et al. 2016, PASP, 128, 124501

Smith, J. C., Stumpe, M. C., Jenkins, J. M., et al. 2017, Kepler Science Document, 8

Soderblom, D. R., Hillenbrand, L. A., Jeffries, R. D., Mamajek, E. E., & Naylor, T. 2014, Protostars and Planets VI, 219

Stauffer, J. R., Hartmann, L. W., Prosser, C. F., et al. 1997, ApJ, 479, 776

Stephenson, C. B. 1959, PASP, 71, 145

Theano Development Team. 2016, arXiv e-prints, abs/1605.02688

Thompson, S. E., Coughlin, J. L., Hoffman, K., et al. 2018, ApJS, 235, 38

Tofflemire, B. M., Rizzuto, A. C., Newton, E. R., et al. 2021, AJ, 161, 171

Vogt, S. S., Allen, S. L., Bigelow, B. C., et al. 1994, SPIE Conference Series, ed. D. L. Crawford & E. R. Craine, Vol. 2198

Yee, S. W., Petigura, E. A., & von Braun, K. 2017, ApJ, 836, 77

Zari, E., Hashemi, H., Brown, A. G. A., Jardine, K., & de Zeeuw, P. T. 2018, A&A, 620, A172

Zhou, G., Quinn, S. N., Irwin, J., et al. 2021, AJ, 161, 2

Table 1. Priors and posteriors for Kepler-1643 transit model with local polynomials removed.

Param.	Unit	Prior	Median	Mean	Std. Dev.	3% HDI	97% HDI	ESS	$\hat{R}-1$
P	d	$\mathcal{N}(5.34264; 0.01000)$	5.3426257	5.3426258	0.0000101	5.3426071	5.3426454	7884	1.1e-03
$t_0^{(1)}$	d	$\mathcal{N}(134.38100; 0.02000)$	134.3820412	134.3820408	0.0011172	134.3798834	134.3840798	7390	3.7e-04
$\log R_{\rm p}/R_{\star}$	–	$\mathcal{U}(-6.215; 0.000)$	-3.68806	-3.68934	0.02072	-3.72788	-3.65275	4449	-7.8e-05
b	–	$\mathcal{U}(0; 1 + R_{\rm p}/R_{\star})$	0.5825	0.5781	0.0514	0.4848	0.6734	4705	1.9e-04
u_1	–	Kipping 2013	0.257	0.294	0.214	0.000	0.678	5324	7.9e-04
u_2	–	Kipping 2013	0.324	0.314	0.324	-0.257	0.880	4908	8.4e-04
$R_{\star}$	$R_{\odot}$	$\mathcal{N}(0.855; 0.044)$	0.851	0.851	0.045	0.766	0.933	7473	7.2e-04
$\log g$	cgs	$\mathcal{N}(4.502; 0.035)$	4.507	4.507	0.035	4.442	4.576	6530	-1.4e-04
$\log \sigma_f$	–	$\mathcal{N}(\log\langle\sigma_f\rangle; 2.000)$	-8.520	-8.520	0.019	-8.556	-8.486	7966	2.1e-04
$\langle f \rangle$	–	$\mathcal{N}(1.000; 0.100)$	1.0000	1.0000	0.0000	1.0000	1.0000	7488	3.2e-04
$R_{\rm p}/R_{\star}$	–	–	0.025	0.025	0.001	0.024	0.026	4449	-7.8e-05
$\rho_{\star}$	g cm^{-3}	–	1.943	1.953	0.191	1.603	2.313	6081	9.4e-05
$R_{\rm p}$	$R_{\rm Jup}$	–	0.207	0.207	0.012	0.184	0.231	6326	2.5e-04
$R_{\rm p}$	$R_{\rm Earth}$	–	2.32	2.32	0.135	2.062	2.589	6326	2.5e-04
$a/R_{\star}$	–	–	14.312	14.322	0.465	13.487	15.228	6081	8.2e-05
$\cos i$	–	–	0.041	0.040	0.005	0.032	0.049	4929	2.4e-04
T_{14}	hr	–	2.408	2.409	0.061	2.304	2.527	4774	5.3e-04
T_{13}	hr	–	2.232	2.233	0.070	2.109	2.362	4561	6.2e-04

NOTE— ESS refers to the number of effective samples. $\hat{R}$ is the Gelman-Rubin convergence diagnostic. Logarithms in this table are base-e. $\mathcal{U}$ denotes a uniform distribution, and $\mathcal{N}$ a normal distribution. Many of the T_{13} statistics may be `nan` in the event of a grazing transit. (1) The ephemeris is in units of BJKD (BJDTDB-2454833).

APPENDIX

A. TABLE OF CANDIDATE RSG-5 AND CH-2 MEMBERS

Gaia source lists and abbreviated info. Include rotation periods.

B. TABLE OF TRANSIT FIT PARAMETERS

Tables 1, 2, 3 give the full set of fitted and derived parameters from the model described in Section 4.2. Priors and convergence statistics are also listed.

Table 2. Priors and posteriors for KOI-7368 transit model with local polynomials removed.

Param.	Unit	Prior	Median	Mean	Std. Dev.	3% HDI	97% HDI	ESS	$\hat{R}-1$
P	d	$\mathcal{N}(6.84294; 0.01000)$	6.8430344	6.8430341	0.0000125	6.8430107	6.8430574	10045	6.5e-05
$t_0^{(1)}$	d	$\mathcal{N}(137.06000; 0.02000)$	137.0463023	137.0463315	0.0014043	137.0436532	137.0489229	10303	9.2e-05
$\log R_{\mathrm{p}}/R_\star$	–	$\mathcal{U}(-4.605; 0.000)$	-3.76025	-3.76299	0.03062	-3.81932	-3.70774	4043	6.3e-04
b	–	$\mathcal{U}(0; 1+R_{\mathrm{p}}/R_\star)$	0.5077	0.4999	0.0641	0.3797	0.6115	4434	3.5e-04
u_1	–	Kipping 2013	0.976	0.953	0.267	0.425	1.422	5809	-5.6e-05
u_2	–	Kipping 2013	-0.191	-0.158	0.308	-0.661	0.421	4387	2.6e-04
$R_\star$	$R_\odot$	$\mathcal{N}(0.876; 0.035)$	0.874	0.874	0.036	0.804	0.938	9902	7.3e-04
$\log g$	cgs	$\mathcal{N}(4.499; 0.030)$	4.503	4.502	0.030	4.445	4.557	7527	2.7e-05
$\log \sigma_f$	–	$\mathcal{N}(\log\langle\sigma_f\rangle; 2.000)$	-8.314	-8.314	0.012	-8.337	-8.292	10636	1.3e-03
$\langle f\rangle$	–	$\mathcal{N}(1.000; 0.100)$	1.0000	1.0000	0.0000	1.0000	1.0000	9742	-2.9e-04
$R_{\mathrm{p}}/R_\star$	–	–	0.023	0.023	0.001	0.022	0.025	4043	6.3e-04
$\rho_\star$	g cm^{-3}	–	1.872	1.878	0.151	1.593	2.159	6829	3.4e-04
R_{p}	R_{Jup}	–	0.198	0.198	0.011	0.177	0.218	5676	2.8e-04
R_{p}	R_{Earth}	–	2.219	2.219	0.123	1.984	2.444	5676	2.8e-04
$a/R_\star$	–	–	16.671	16.677	0.447	15.863	17.542	6829	3.3e-04
$\cos i$	–	–	0.030	0.030	0.004	0.022	0.038	4518	5.4e-04
T_{14}	hr	–	2.789	2.792	0.075	2.651	2.928	4845	5.0e-04
T_{13}	hr	–	2.619	2.622	0.085	2.470	2.779	4575	3.1e-04

NOTE— ESS refers to the number of effective samples. $\hat{R}$ is the Gelman-Rubin convergence diagnostic. Logarithms in this table are base-e. $\mathcal{U}$ denotes a uniform distribution, and $\mathcal{N}$ a normal distribution. Many of the T_{13} statistics may be `nan` in the event of a grazing transit. (1) The ephemeris is in units of BJKD (BJDTDB-2454833).

Table 3. Priors and posteriors for KOI-7913 A transit model with local polynomials removed.

Param.	Unit	Prior	Median	Mean	Std. Dev.	3% HDI	97% HDI	ESS	$\hat{R}-1$
P	d	$\mathcal{N}(24.27838; 0.01000)$	24.2785532	24.2785706	0.0002630	24.2781117	24.2790852	4413	1.5e-03
$t_0^{(1)}$	d	$\mathcal{N}(154.51300; 0.05000)$	154.5121202	154.5124405	0.0062825	154.4998424	154.5237474	5612	6.0e-04
$\log R_{\mathrm{p}}/R_\star$	–	$\mathcal{U}(-5.298; 0.000)$	-3.59884	-3.60184	0.04605	-3.68852	-3.51878	4290	5.6e-04
b	–	$\mathcal{U}(0; 1+R_{\mathrm{p}}/R_\star)$	0.3120	0.2985	0.1526	0.0045	0.5232	2373	1.8e-03
u_1	–	Kipping 2013	0.267	0.337	0.281	0.000	0.862	4491	-6.1e-05
u_2	–	Kipping 2013	0.209	0.229	0.325	-0.309	0.860	5935	7.0e-04
$R_\star$	$R_\odot$	$\mathcal{N}(0.790; 0.049)$	0.788	0.788	0.049	0.699	0.881	6847	2.8e-04
$\log g$	cgs	$\mathcal{N}(4.523; 0.043)$	4.526	4.527	0.042	4.450	4.606	5714	6.6e-04
$\log \sigma_f$	–	$\mathcal{N}(\log\langle\sigma_f\rangle; 2.000)$	-7.197	-7.197	0.019	-7.230	-7.161	6976	1.4e-04
$\langle f\rangle$	–	$\mathcal{N}(1.000; 0.100)$	1.0000	1.0000	0.0000	1.0000	1.0000	6998	2.8e-04
$R_{\mathrm{p}}/R_\star$	–	–	0.027	0.027	0.001	0.025	0.030	4290	5.6e-04
$\rho_\star$	g cm^{-3}	–	2.199	2.213	0.250	1.781	2.705	5357	5.6e-04
R_{p}	R_{Jup}	–	0.209	0.209	0.016	0.179	0.238	4882	1.3e-03
R_{p}	R_{Earth}	–	2.343	2.343	0.179	2.006	2.668	4882	1.3e-03
$a/R_\star$	–	–	40.920	40.949	1.539	38.143	43.845	5357	6.6e-04
$\cos i$	–	–	0.008	0.007	0.004	0.000	0.013	2344	1.9e-03
T_{14}	hr	–	4.394	4.396	0.207	3.980	4.758	3952	5.6e-04
T_{13}	hr	–	4.133	4.132	0.222	3.715	4.548	3632	7.6e-04

NOTE— ESS refers to the number of effective samples. $\hat{R}$ is the Gelman-Rubin convergence diagnostic. Logarithms in this table are base-e. $\mathcal{U}$ denotes a uniform distribution, and $\mathcal{N}$ a normal distribution. Many of the T_{13} statistics may be `nan` in the event of a grazing transit. (1) The ephemeris is in units of BJKD (BJDTDB-2454833).